

# Microstructural Evolution of Udimet 720 Superalloy

I. Calliari, M. Magrini, and M. Dabalà

(Submitted 26 November 1997; in revised form 15 September 1998)

**The microstructural evolution of the nickel-base superalloy Udimet 720 (Special Metals Corp., New Hartford, NY) aged at 850 °C for 1000 to 2000 h is presented. After aging, the  $\gamma$  precipitates change from cubic to globular morphology. Secondary  $\gamma$  particles and topologically close-packed phases were not found. The  $\gamma$  mean diameter increases with aging times, following the Lifshitz-Wagner model. The experimented aging times have no strong effects on mechanical properties of Udimet 720.**

**Keywords** heat treatments, nickel-base superalloys, phase extraction, scanning electron microscopy, transmission electron microscopy, Udimet 720

## Introduction

The term superalloy is normally used to describe multiphase and multicomponent alloys based on nickel, cobalt, or iron. The most important properties of the superalloys are long-time strength at high temperatures (above 650 °C) and resistance to hot corrosion and erosion. Nickel-base superalloys are widely employed in gas turbine engines (Ref 1) because of their good behavior at high temperature with respect to creep (Ref 2), fatigue, corrosion, fracture toughness, and microstructural stability. These properties are due to the mixture of face-centered cubic (fcc)-ordered  $\gamma$  precipitate ( $A_3B$  type) embedded in the  $\gamma$  matrix, strength improving with increasing  $\gamma$  volume fraction.

Carbides are also present, particularly MC,  $M_{23}C_6$ , and  $M_6C$ ; the topologically close-packed (TCP) phases are undesirable because of their negative effect on the mechanical strength. During services in gas turbines, the strong variations in superalloy microstructure induced by aging can cause a reduction in creep strength properties. As this reduction may limit the residual life of a component part, an investigation into microstructural changes in aging is justified.

This article describes the microstructural evolution of the nickel-base superalloy Udimet 720 (Special Metals Corp., New Hartford, NY) (Ref 3), aged at 850 °C for 1000 to 2000 h. This alloy is increasingly used in the form of forged rotor blades in land-based gas turbines (Ref 4, 5). Heat treatments for the precipitation-strengthened alloy Udimet 720 generally consist of a solution treatment in inert atmosphere (1170 °C for 4 h), followed by stabilization (1080 °C for 4 h) and a two-step aging (850 °C for 24 h, 760 °C for 16 h).

**I. Calliari, M. Magrini, and M. Dabalà**, Department of Mechanical and Management Innovation, University of Padua, Via Marzolo, 9, 35141 Padova, Italy. Contact e-mail: calliari@ux1.unipd.it.

**Table 1 Chemical composition of Udimet 720**

Alloy	Composition, wt%									
	Cr	Co	Mo	W	Ti	Al	C	B	Zr	Ni
Udimet 720	18.00	14.70	3.00	1.25	5.00	2.50	0.035	0.033	0.030	55.45

## Materials and Methods

The chemical composition of the cast nickel-base alloy Udimet 720 examined in this study is given in Table 1.

Aging at 850 °C for 1000 h (sample 2), 1250 h (sample 3), 1500 h (sample 4), 1750 h (sample 5), and 2000 h (sample 6) simulated the service. After aging, the microstructural characterization was carried out with optical microscopy (OM), scanning electron microscopy (SEM), and transmission electron microscopy (TEM). To determine the  $\gamma/\gamma'$  weight, a phase extraction was done.

Metallographic specimens were obtained from aged and unaged samples. They were sectioned, mounted, polished, and etched using a Kalling reagent, and then they were electroetched with 2%  $CrO_3$  in aqueous solution. An electroetching with 20 mL  $H_3PO_4$  and 80 mL  $H_2O$  was adopted for SEM examination (Ref 1). Though the SEM depth of field permits the examination of specimen overetched by OM, great care was taken to avoid attacking the fine secondary  $\gamma$  (Ref 6).

Thin foils for TEM were prepared from disks of 3 mm diameter, thinned to perforation in a Tenupol (Struers, Denmark) twin-jet electropolisher. A solution of 5% perchloric acid in butylglycol at -15 °C was used as electrolyte, and a voltage of 30 V was applied.

The previously indicated etchants attack the  $\gamma$  solid solution, bringing out the  $\gamma'$  phase. Scanning electron microscopy observations were done in secondary and backscattered modes; TEM micrographs were taken in bright-field mode.

Specimens for phase extraction were first coarse ground and then fine ground to remove oxide layers or corrosion deposits and then weighed.

The dissolution was carried out with an aqueous solution of 1% tartaric acid and 1%  $(NH_4)_2SO_4$ , in aqueous solution with an anodic potential of about 1,000 V referred to the calomel electrode and with a current density less than 10 mA/cm<sup>2</sup>. After ultrasonic treatment, the solution was filtered on a 0.22  $\mu$ m Millipore GSWP filter (Millipore Corp., Bedford, MA).

The x-ray diffraction (XRD) (Cu  $K\alpha$  radiation, D500 Siemens), carried out on the filtered particles, did not reveal traces

of  $\gamma$  phase. The  $\gamma$  fraction was obtained by weight loss, and its chemical composition was determined by atomic absorption spectrometry (AAS).

To investigate  $\gamma$  and secondary phases, a selective solution of particles adhering to the filter was performed with a Berzelius reagent (160 g of  $\text{CuCl}_2 \cdot 2\text{H}_2\text{O}$ , 140 g of KCl, 10 g of tartaric acid in 7.5% HCl aqueous solution). A filtration was carried out with 0.22  $\mu\text{m}$  Millipore GSWP filter, and the particles were submitted to XRD.

The fractions of  $\gamma$  and of secondary phases were determined by weighing. After elimination of Cu by electrolysis at 2 V, the chemical composition of  $\gamma$  was determined by AAS.

## Results and Discussion

Table 2 provides the mean values of microhardness. As the time of service lengthens, the Vickers hardness values decrease. This may be due to the growth of  $\text{M}_{23}\text{C}_6$  and  $\text{M}_6\text{C}$  (Ref

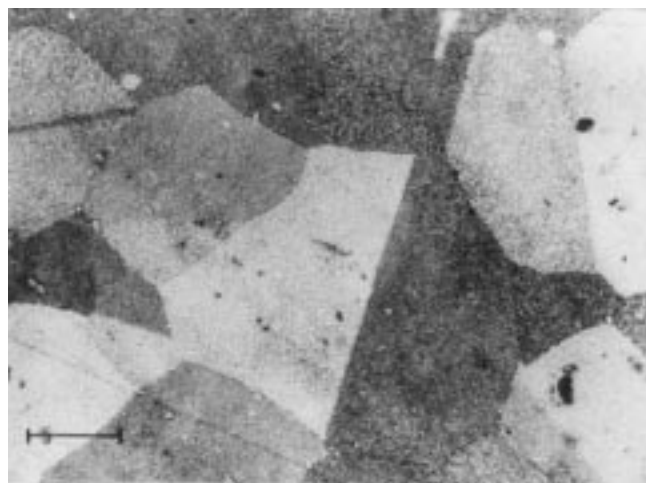


**Fig. 1** Microstructure of an unaged sample (marker = 1 mm), ASTM grain size No. 0

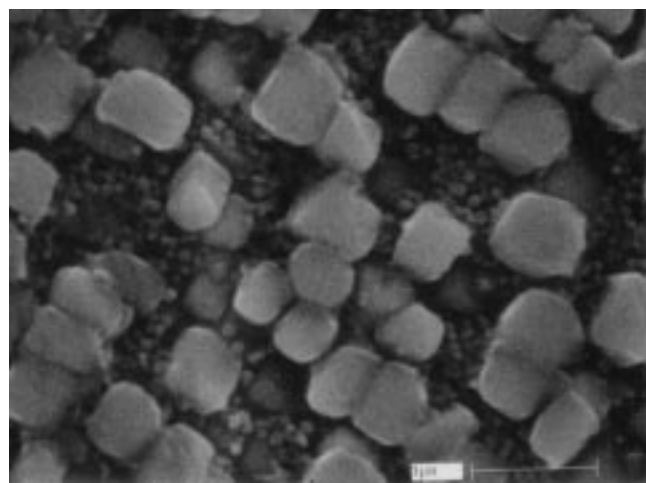


**Fig. 2** SEM image of an unaged sample showing primary and secondary  $\gamma$  phases

1), which deplete the matrix of refractory elements responsible for solid-solution strengthening.

### Optical Microscopy and SEM Examinations

Figure 1 shows the microstructure of sample 1 with heterogeneous grain size of ASTM No. 0. There are also fine precipitates in intergranular and transgranular positions, with preferential alignment parallel to blade axis, in parallel to cooling hole. At grain boundaries and in particular at triple points, zones with lamella morphology of  $\gamma$  eutectic phase, arising from melt cooling, are shown.

A SEM micrograph of an unaged sample is shown in Fig. 2. A cubic primary  $\gamma$  phase and a secondary globular  $\gamma$  phase are evident. The size of the cubic phase is in the 0.5 to 0.6  $\mu\text{m}$  range, without preferential orientation on specific crystalline plane. The globular particles, probably arising from direct cooling from melt, have uniform sizes of about 0.05  $\mu\text{m}$ . The acicular TCP phases, responsible for strong deterioration of mechanical properties, are absent. Carbides are present both in transgranular and intergranular position with MC-type block morphology (Fig. 3).

Figures 4 and 5 show the SEM micrographs of samples aged for 1250 and 2000 h. Both samples have globular primary  $\gamma$  phase with size in 0.35 to 0.8  $\mu\text{m}$  range; even if there is no evidence of secondary  $\gamma$  phase, some globules of about 0.25  $\mu\text{m}$  were found. The precipitate volume fractions seem to be constant as the aging time increases. Carbides are localized at transgranular positions, and the TCP acicular phases are absent (Fig. 6).

**Table 2** Mean values of microhardness in samples at different aging times

Aging time, h	Microhardness, 0.2 HV
0	468
1000	426
1500	419
2000	415

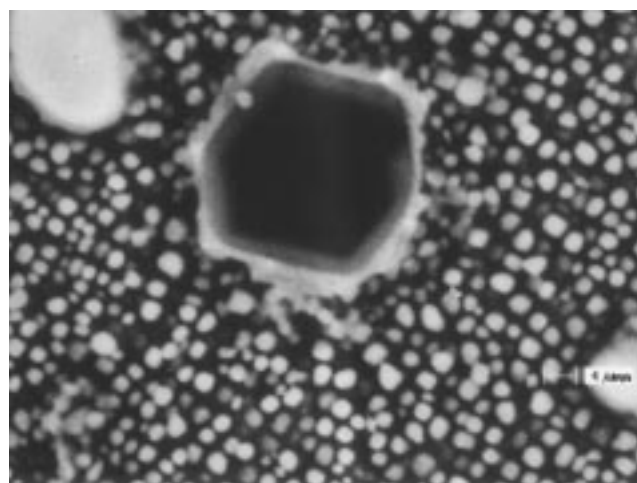


**Fig. 3** Carbides with MC-type morphology (SEM image, unaged sample)

From the reported results, one may deduce that the adopted aging times are probably too short to induce remarkable microstructural changes; still with these aging times, the following effects have been found:

- The evolution of primary  $\gamma$  phase from cubic morphology (typical of unaged material) to globular morphology (typical of aged material)
- In aged samples, the disappearance of secondary  $\gamma$  phase

### Transmission Electron Microscopy Examinations

As seen with SEM, TEM did not reveal strong microstructural modifications in aged samples. The  $\gamma$  phase has cubic (0.6 to 0.7  $\mu\text{m}$ ) and globular (0.4 to 0.5  $\mu\text{m}$ ) morphology, mainly distributed as single particles with few aggregates (Fig. 7, 8). The transition of  $\gamma$  from spherical to cubic shape occurs when  $\gamma$  dimensions are larger than 0.5  $\mu\text{m}$ . This value is higher than those reported (about 0.3  $\mu\text{m}$ ) (Ref 1, 7) for other types of superalloys. This difference may be due to the  $\gamma$ - $\gamma'$  misfit: if it is about 0, as in Udimet 720, the  $\gamma$ -elastic deformation is small and the precipitates have to be large enough to avoid shape deformation.

Secondary  $\gamma$  and acicular TCP phases were not evidenced by TEM investigation. The resolution of TEM micrographs has allowed the measurement of the mean diameter of  $\gamma$  precipitates in samples 2 and 5. Sample 2 has a  $\gamma$  mean diameter of 490 nm (standard deviation, SD = 105 nm, number of values,  $N = 150$ ), while sample 5 has a mean diameter of 620 nm (S.D. = 106 nm,  $N = 160$ ), values that confirm the growth of  $\gamma$  phase with aging.

**Table 3 Weight fractions of superalloy phases**

Sample	$\gamma$ phase, %	$\gamma$ + secondary phase, %	$\gamma$ phase, %	Secondary phase, %
1	62.3	37.7	36.5	1.2
2	61.9	38.1	37.2	0.9
3	62.2	37.8	36.0	1.3
4	61.4	39.0	37.2	1.7
5	62.3	37.5	36.6	1.0
6	60.7	39.3	37.9	1.4

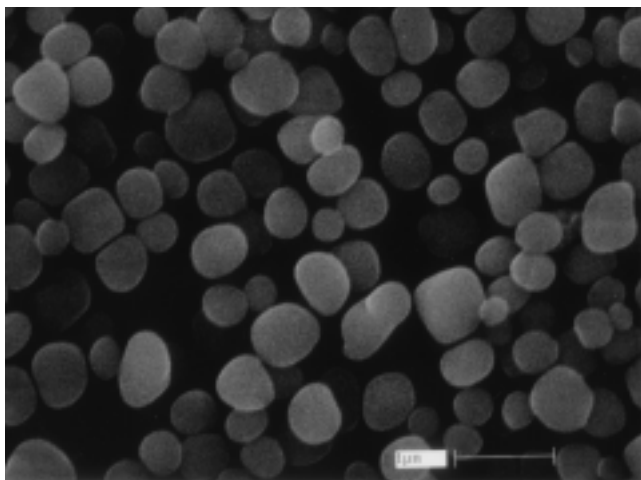


**Fig. 4** SEM image of sample 3 with globular  $\gamma$  phase

In order to apply the Lifshitz-Wagner criteria (Ref 8, 9), the sample 5 diameter value was assumed to be determined with more accuracy than the sample 2 diameter (160 data against 150). Thus, the calculated mean diameter for sample 2 is 514 nm, the difference from the experimental value is about 5%. One may conclude that the model adequately describes the kinetic of  $\gamma$  growth.

### Phase Extraction

Table 3 reports the weight fractions (mean values of two determinations) of the superalloy phases obtained with selective extractions. The sum of the fractions of the different phases is almost constant in all samples. The mean value for  $\gamma$  fraction is 61.8%, while that for  $\gamma'$  and the secondary phase is 38.2%. The mean value of weight fractions of  $\gamma$  phase, determined after selective extraction with Berzelius reagent, is 37%. The XRD patterns of secondary-phase particles show that titanium carbide and  $\text{M}_{23}\text{C}_6$  carbide (probably  $\text{Cr}_{21}\text{Mo}_2\text{C}_6$ ) are present in all samples. The data reported in Table 3 do not show significant variations in weight fractions with increase of aging

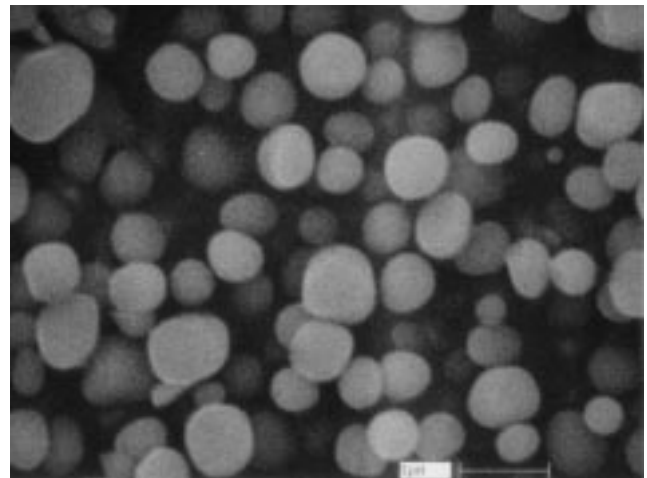


**Fig. 5** SEM image of sample 6 with globular  $\gamma$  phase

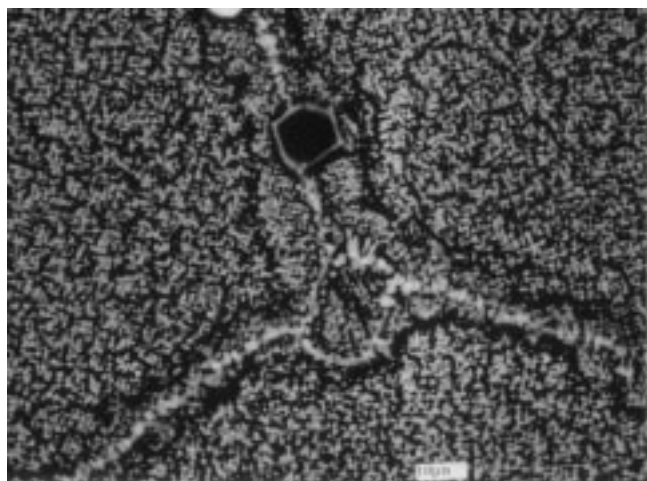
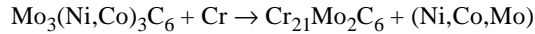


**Fig. 6** SEM (BSE) image of sample 5 with carbides at transgranular positions

time, as already reported for similarly employed superalloys (Ref9).

Tables 4 and 5 report the compositions (at.%) of  $\gamma$  and  $\gamma'$  phases; these data were obtained with AAS analysis of solutions from selective extractions.

The  $\gamma$  phase composition is almost constant with increasing aging time, apart from the chromium decrease and the nickel increase. The low content of chromium after long aging times may be due to the formation of precipitated carbides. One can suppose that, after a long exposure to high temperature, the following reaction might take place:



As chromium has a high number of electronic vacancies (4.66), a lowering of its content improves  $\gamma$  phase stability in

contrast with the TCP precipitation caused by the decrease in the electronic vacancies mean number  $N_{\text{vm}}$ . This value can be determined with the PHACOMP method developed by Sims, starting from the atomic matrix composition. Figure 10 shows the  $N_{\text{vm}}$  values trend as a function of aging time.

Regarding  $\gamma'$  phase, no significant variations in chemical composition have been evidenced. Although there is no universally recognized stoichiometry of  $\gamma'$  phase, several formulas have been proposed. Nickel and aluminum, which form the intermetallic compound  $\text{Ni}_3\text{Al}$ , can be substituted by other alloy elements, such as cobalt, tungsten, titanium, chromium, and molybdenum.

Cobalt and tungsten may substitute nickel, titanium may substitute aluminum, while chromium and molybdenum may substitute both elements. Three stoichiometries for  $\gamma'$  Udimet 720 alloy have been formulated:

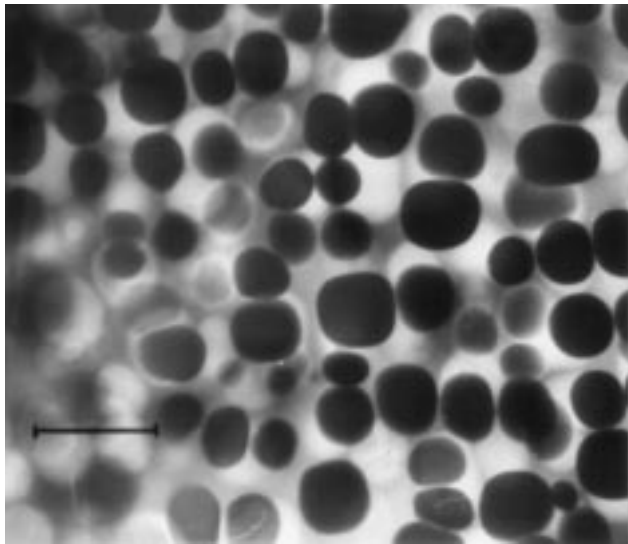
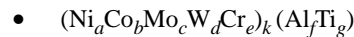


**Fig. 7** TEM (BF) image of sample 2 with globular and cubic  $\gamma'$  phase

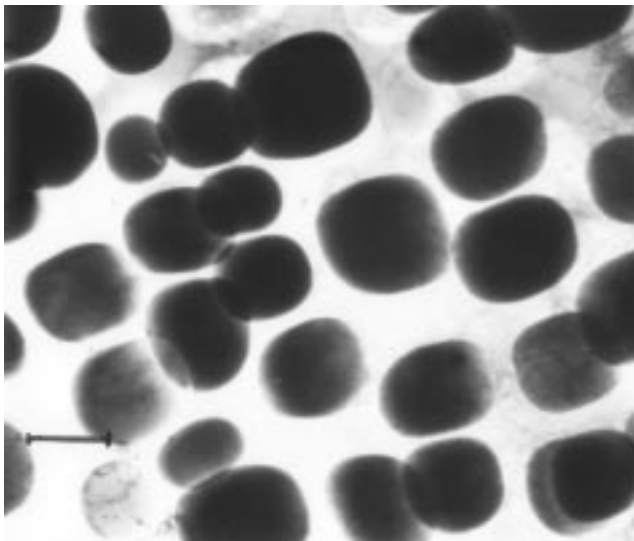


**Fig. 8** TEM (BF) images of sample 5 with globular  $\gamma'$  phase

**Table 4** Compositions of  $\gamma$  phase

Element	Aging time, h					
	0	1000	1250	1500	1750	2000
Ni	43.70	44.60	45.22	46.26	45.97	47.84
Co	17.65	17.08	18.41	18.60	18.71	18.49
Cr	34.62	33.58	32.38	33.07	30.65	29.60
Mo	3.46	4.19	3.52	3.35	4.15	3.67
Ti	0.56	0.54	0.48	0.21	0.50	0.45

**Table 5** Compositions of  $\gamma'$  phase

Element	Aging time, h					
	0	1000	1250	1500	1750	2000
Ni	67.94	67.88	67.61	65.82	67.38	67.68
Co	5.03	4.98	4.77	4.90	4.93	5.32
Cr	2.83	2.56	2.56	2.78	2.70	2.63
W	1.84	1.71	1.57	1.78	1.84	2.10
Al	10.11	10.07	10.69	10.87	10.21	9.72
Mo	0.88	0.64	0.75	0.91	0.92	0.72
Ti	11.40	12.26	12.05	12.93	11.75	11.83

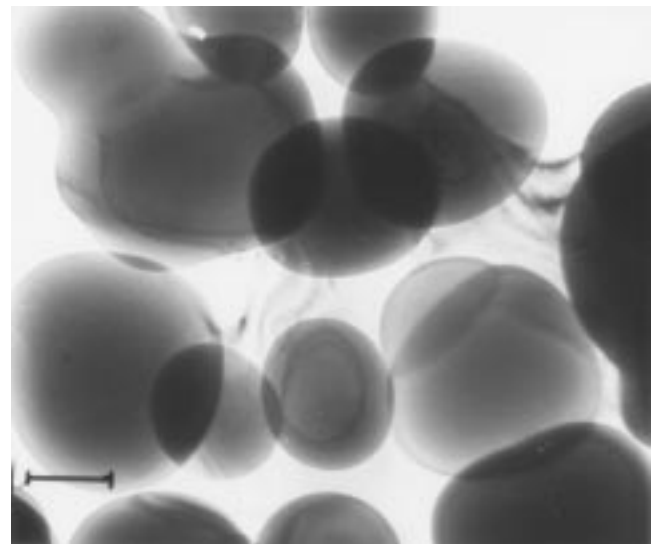


**Fig. 9** TEM (BF) images of sample 5 with globular  $\gamma'$  phase



**Fig. 10** Trend of the  $N_{vm}$  values as a function of aging time

- $(Ni_aCo_bMo_cW_d)_k(Al_fTi_gCr_e)$
- $(Ni_aCo_bMo_cW_dCr_e)_3(Al_fTi_gCr_e)$

From Table 5, the authors suggest hypothesis 2 as the most probable because the sum of the titanium, chromium, and aluminum atomic percentages is about 25, giving a  $k$  stoichiometric coefficient equal to 3.

## Conclusions

The investigation of the aging influence on nickel-base superalloy Udimet 720 put in evidence the following microstructural variations:

- $\gamma$  precipitates change from cubic to globular morphology.
- Secondary  $\gamma$  particles are not found in aged samples.

Topologically close-packed phases are not found in any of the samples, so the mechanical properties are not strongly influenced by aging.

In samples 2 and 5 (1000 and 1750 h)  $\gamma$  precipitates have cubic (0.65  $\mu\text{m}$  size) and spherical (0.35  $\mu\text{m}$  size) shapes, respectively.

The  $\gamma$  mean diameter increases with aging, and the growth kinetics follows the Lifshitz-Wagner model.

The phase selective extraction data show that aging has no effect on the weight fractions of the alloy phases. The variations in the chemical composition phase are rather modest, with a constant decrease in the chromium content.

This chromium trend keeps the mean number of matrix electronic vacancies lower than the critical limit so the precipitation of the TCP phases is avoided. Following the more probable stoichiometric hypothesis of  $\gamma$  composition, chromium tends to be isomorphic with aluminum.

From the above results, one can conclude that, within the adopted aging times, the mechanical properties of Udimet 720 did not undergo significant variations.

## References

1. E.F. Bradley, *Superalloys: A Technical Guide*, ASM International, 1988
2. R.W. Evans and B. Wilshire, Creep Behaviour of Superalloy Blade Materials, *Mater. Sci. Technol.*, Vol 3, 1987, p 701-705
3. "Udimet 720—A New Alloy for Land Gas Turbines," Data sheet, Special Metals Corp., New Hartford, NY, 1978
4. H. Puschnik, G. Zeiler, J. Fladischer, W. Eber, and K.H. Keienburg, Udimet 720 Turbine Blades—Production and Properties, *Metall. Ital.*, Vol 82 (No. 5), 1990, p 473-476
5. G.W. Meetham, Keynote Lecture—Material for Advanced Gas Turbines, *High Temperature Alloys for Gas Turbines and Other Applications 1986*, W. Betz et al., Ed., D. Reidel Publishing, Dordrecht, 1986, p 1-18
6. S.T. Wlodek, SEM Metallography of Superalloys, *Microstructural Sciences*, T.A. Place, J.D. Braun, W.E. White, and G.F. Vander Voort, Ed., Vol 18, 1990, p 407-429
7. F. Shubert, Temperature and Time Dependent Transformations; Application to Heat Treatment of High Temperature Alloys, *Phase Stability in High Temperature Alloys*, W. Guttmann, Ed., Applied Science Publishers, 1981, p 119
8. M. Lifshitz and V.V. Slyozov, The Kinetics of Precipitation from Supersaturated Solid Solution, *J. Phys. Chem. Solids*, Vol 19, 1961, p 35-50
9. Y. Yoshioka, N. Okabe, T. Okamura, D. Saito, K. Fujijama, and H. Kashiwaya, Service Temperature Estimation for Heavy Duty Gas Turbine Buckets Based on Microstructure and Change, *Superalloys 1996*, R.D. Kissinger, Ed., The Minerals, Metals and Materials Society, 1996, p 173-179
10. C.T. Sims, The Occurrence of Topologically Close-Packed Phases, *The Superalloys*, C.T. Sims and W.C. Hagel, Ed., J. Wiley & Sons, NY, 1972, p 259-284